

A Single-Molecule Study of RNA Catalysis and Folding

Xiaowei Zhuang,^{1*} Laura E. Bartley,^{2*} Hazen P. Babcock,¹
Rick Russell,² Taekjip Ha,¹ Daniel Herschlag,^{2†} Steven Chu^{1†}

Using fluorescence microscopy, we studied the catalysis by and folding of individual *Tetrahymena thermophila* ribozyme molecules. The dye-labeled and surface-immobilized ribozymes used were shown to be functionally indistinguishable from the unmodified free ribozyme in solution. A reversible local folding step in which a duplex docks and undocks from the ribozyme core was observed directly in single-molecule time trajectories, allowing the determination of the rate constants and characterization of the transition state. A rarely populated docked state, not measurable by ensemble methods, was observed. In the overall folding process, intermediate folding states and multiple folding pathways were observed. In addition to observing previously established folding pathways, a pathway with an observed folding rate constant of 1 per second was discovered. These results establish single-molecule fluorescence as a powerful tool for examining RNA folding.

Virtually all knowledge of chemical processes has been deduced from ensemble measurements. This has led us to think of molecular processes as well-ordered sets of events. However, single-molecule studies of polymer dynamics have led to the discovery that identical molecules exposed to the same conditions follow different paths to a new equilibrium state (1). Biological processes, such as protein and RNA folding, and multicomponent processes, such as transcription and translation, are also likely to involve a rich set of kinetic paths and transient states. These complex processes may be understood more clearly by single-molecule studies that allow one to look beyond ensemble averages and observe the distributions and time trajectories of individual molecules. Single-molecule experiments on ion channels (2), motor proteins (3–6), enzymes (7), and other proteins (8–11) have provided insights into the molecular mechanisms of their biological functions.

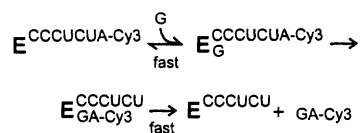
Here, we explore RNA folding, using a single-molecule approach. RNA plays a central role in cellular processes such as splicing and translation, performing a variety of functions including ligand binding, structural scaffolding, and catalysis (12). These functions are largely determined by the complex and specific three-dimensional structures that functional RNA molecules adopt. However, systematic efforts toward understanding the folding of large RNA molecules began only recently (13–21). In particular, the *Tetrahymena* ribozyme is an intensely studied catalytic RNA of ~400 nucle-

otides, derived from a self-splicing group I intron (22). It folds to the native structure through multiple intermediate states and pathways (13–18). Here, we report a single-molecule study of the catalysis by and folding of the *Tetrahymena* ribozyme.

For the single-molecule experiments, we extended the L-21 Sca I form of the *Tetrahymena* ribozyme at its 3'-end and annealed it to a complementary oligonucleotide tether with a 5'-biotin (Fig. 1) (23), allowing the ribozyme to be immobilized to a surface via a streptavidin-biotin interaction (24). Fluorescent dyes were attached to the ribozyme as shown in Fig. 1: a Cy3 dye at the 3'-end of the oligonucleotide substrate (S) bound to the ribozyme and, when required, a Cy5 dye at the 3'-end of the tether (23). Single ribozyme molecules were detected using a total internal reflection microscope or a scanning confocal microscope (25). The buffer conditions we used are described in (23).

Surface-immobilization greatly facilitates measuring the temporal behavior of individual molecules while solution conditions are changed. However, immobilization can adversely affect the properties of the molecules. It is therefore necessary to thoroughly characterize the functional integrity of surface-immobilized molecules. This was possible for the *Tetrahymena* ribozyme because of the extensive kinetic and thermodynamic framework established for its enzymatic reaction (26).

The ribozyme catalyzes the cleavage of S by guanosine (G) (Scheme 1)



Scheme 1.

To measure this reaction at the single-molecule level, we added G to the surface-immobilized ribozyme molecules with bound S (23). After rapid binding of G, cleavage occurs and the Cy3-labeled cleavage product is released from the ribozyme (23), leading to the disappearance of fluorescence of individual molecules. Figure 2 shows the cleavage rate constants obtained using this method at several G concentrations, together with results obtained from ensemble measurements of the same ribozyme construct free in solution (27). The identical rate constants from the two methods indicate that the ribozyme and the ternary complex of ribozyme·S·G were unperturbed by the surface (28). In addition, the rate constant for release of S from the immobilized ribozyme is similar to that from free ribozyme in solution (23), demonstrating that the ribozyme·S complex is also unperturbed by the surface. We also found the effects of the 3'-extension and dye-labeling on the cleavage reaction and substrate release to be insignificant (23). The fact that the rate and equilibrium constants that constitute the catalytic cycle of the ribozyme were not significantly changed by surface-immobilization or dye-labeling indicates that the properties of the ribozyme are accurately reflected despite the modifications present in the single-molecule experiments.

In the following, we will explore two aspects of ribozyme folding, P1 docking and overall folding, using fluorescence resonance energy transfer (FRET) at the single-molecule level (29–32). Two fluorescent dyes, Cy3 (donor) and Cy5 (acceptor), are attached to specific sites on the ribozyme as shown in Fig. 1. Because of the dipolar interaction between the donor and acceptor, the excitation energy of the donor can be transferred to the acceptor with the efficiency depending on their distance and orientations. Thus, the FRET efficiency can report on conformational changes of the host ribozyme (33).

We first probed a local folding transition in which the P1 duplex formed between the ribozyme and S reversibly docks into the active core of the ribozyme (Fig. 3A) (34, 35). P1 docking is a relatively simple transition between secondary and tertiary structure, because the tertiary structure of the core into which P1 docks is largely preformed (36, 37). Thus, this transition may be particularly amenable to in-depth study and can provide general insight into the mechanism by which the tertiary structure of RNA forms.

The upper panel of Fig. 3B shows the FRET time trajectory of a single ribozyme molecule. The FRET value fluctuates between two distinct levels. The model of the ribozyme tertiary structure (38) and the crosslinking between P1 and the ribozyme core (39, 40) suggests that the distance between the donor and the acceptor decreases

¹Department of Physics, Stanford University, Stanford, CA 94305–4060, USA. ²Department of Biochemistry, B400 Beckman Center, Stanford University, Stanford, CA 94305–5307, USA.

*These authors contributed equally to this work.
†To whom correspondence should be addressed. E-mail: herschla@cmgm.stanford.edu (D.H.) and schu@stanford.edu (S.C.)

from ~7 nm in the undocked state to 1 to 2 nm upon docking (Fig. 3A). We thus assigned the higher FRET value to the docked

state and the lower one to the undocked state. Histograms of dwell times in the two states give the rate constants for docking $k_{\text{dock}} =$

$1.62 \pm 0.08 \text{ s}^{-1}$ and for undocking $k_{\text{undock}} = 0.224 \pm 0.015 \text{ s}^{-1}$ (Fig. 4) (41). The docking equilibrium constant, $K_{\text{dock}} = k_{\text{dock}}/k_{\text{undock}} = 7.2 \pm 0.8$, agrees with the value measured using a well-established ensemble method ($K_{\text{dock}} = 7 \pm 3$) (23), supporting the above FRET level assignments.

As a first step toward understanding the properties that govern the docking transition, we probed whether a specific tertiary contact is formed before or after the highest energy state on the docking reaction coordinate, i.e., the transition state (42). If the contact is formed in the transition state, disruption of the contact will increase the free energy difference between the transition state and the undocked state, thus decreasing the rate of docking. Alternatively, if the contact is formed after traversing the transition state, its disruption will destabilize the docked state but leave the transition state unaffected. This will accelerate undocking without affecting the rate of docking.

Previous studies have shown that the 2'-hydroxyl group of residue U-3 on S (Fig. 1) makes tertiary contact with the ribozyme core in the docked state (43). Replacement of this group with methoxy to give a modified substrate, -3mS, greatly destabilizes the docked state (40, 44). The lower panel of Fig. 3B shows a FRET time trace of the ribozyme with -3mS. The histograms of the dwell times in the undocked and docked states give $k_{\text{dock}} = 1.25 \pm 0.06 \text{ s}^{-1}$ and $k_{\text{undock}} = 11.5 \pm 1.0 \text{ s}^{-1}$ (Fig. 4). The equilibrium constant, $K_{\text{dock}} = 0.109 \pm 0.015$, is consistent with previous ensemble measurements (40), further confirming the FRET level assignments. The small value of K_{dock} means that the docked state is rarely populated, so that k_{dock} and k_{undock} cannot typically be measured by ensemble methods.

Comparison of the rate constants for docking and undocking with all-ribose S and with -3mS reveals that k_{dock} is unaffected,

Fig. 1. The secondary structure of the *Tetrahymena* ribozyme used here. The thin line and the six residues, GGAGGG, represent the L-21 Sca I ribozyme. The thick line represents the extension of the 3'-end of the L-21 Sca I ribozyme, which is base-paired with a complementary DNA oligonucleotide with a 5'-biotin. The RNA oligonucleotide substrate S (CCCUCU_x) labeled with a fluorescent dye, Cy3, binds to the ribozyme to form the P1 duplex. In the cleavage experiments, $x = 1$, and in the docking and folding experiments, $x = 4$. The fluorescent dye Cy5 on the 3'-end of the DNA tether was not present in the cleavage experiments. The residues and duplexes (P1 through P9.2) are numbered on the basis of the *Tetrahymena* self-splicing intron.

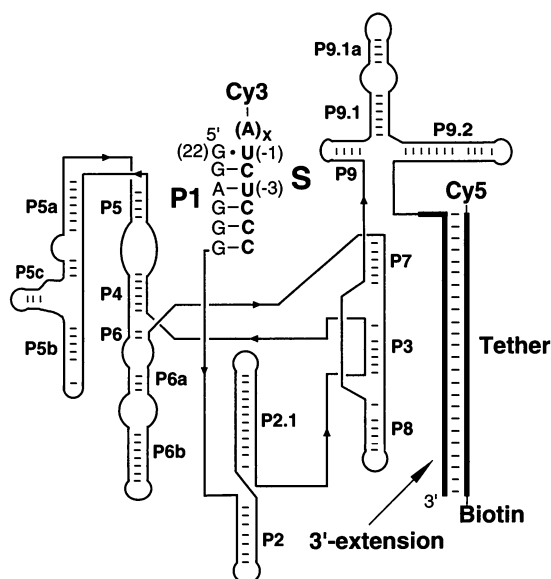


Fig. 2. A comparison of ribozyme reaction kinetics determined from single-molecule measurements (●) and from ensemble measurements (○). The solid line is a fit to the single-molecule data by $k = k_{\text{max}}[G]/(K_{1/2}^G + [G])$, with $k_{\text{max}} = 0.21 \pm 0.01 \text{ s}^{-1}$ and $K_{1/2}^G = 0.26 \pm 0.04 \text{ mM}$. The dashed line is the same fit to the ensemble data, with $k_{\text{max}} = 0.21 \pm 0.01 \text{ s}^{-1}$ and $K_{1/2}^G = 0.30 \pm 0.05 \text{ mM}$. (Inset) A single-molecule measurement of cleavage reaction at 1 mM G: the number of remaining fluorescent molecules (N) versus time. The initial lag (~1 s) is due to a delay between the initiation of cleavage buffer and its arrival at the sample. The line is an exponential fit, giving the cleavage rate constant $k = 0.16 \text{ s}^{-1}$. A real-time movie showing the cleavage reaction and the control experiment of photobleaching is available (23).

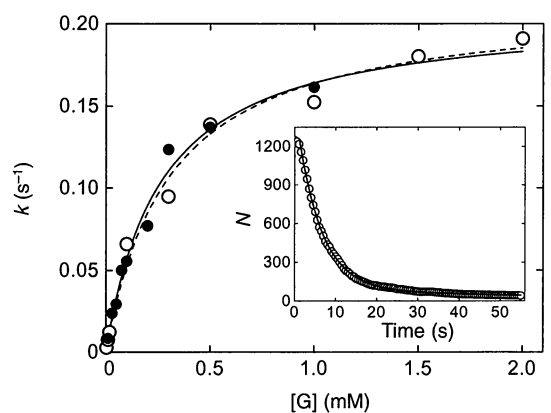
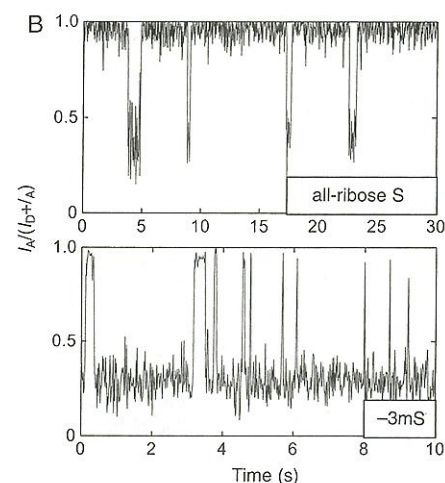
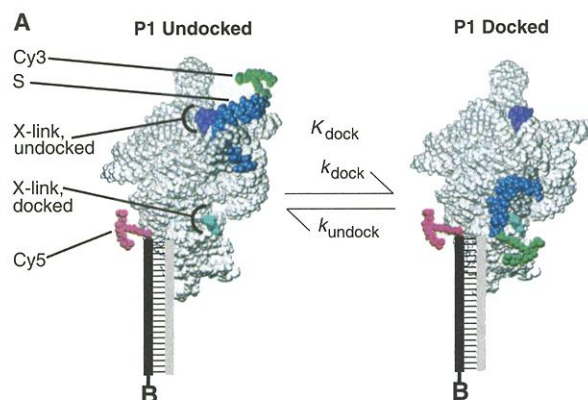


Fig. 3. (A) Docking of the P1 duplex in the context of the medium-resolution model of the *Tetrahymena* ribozyme (38). The P1 duplex between S (blue) and the 3'-end of ribozyme (gray) reversibly docks into the ribozyme (light gray). With an azidophenacyl group coupled at the 5'-end of the P1 duplex (residue G22), crosslinking occurs at different positions in the undocked (purple) and docked states (cyan) (39, 40). FRET between Cy3 (green) on S and Cy5 (red) on the tether (black) gives a signal for docking. (B) FRET time traces from single ribozyme molecules showing P1 docking and undocking. FRET is defined as $I_A/(I_D + I_A)$, where I_D and I_A are the fluorescence signals from donor and acceptor, respectively. The docked and undocked states give FRET values of ~0.9 and ~0.3, respectively. The same FRET values were observed with the Cy5 attached after a single A residue (Fig. 1, $x = 1$).



whereas k_{undock} is increased 50-fold by the -3m modification. Thus, the tertiary contact between the 2'-hydroxyl group of residue U-3 on S and the ribozyme core is not yet formed in the docking transition state, but forms subsequently. These and other data (45) support a preliminary model in which the transition state for docking lacks all tertiary contacts between P1 and the core.

We next probed the overall folding of the ribozyme from an unfolded state with secondary structure. The ribozyme in the unfolded state gave a FRET value of ~ 0.1 (23), much lower than that in the native state (~ 0.9 in the docked state and ~ 0.3 in the undocked state), and thus the FRET signal can be used to examine the overall folding transition. Refolding of the unfolded ribozyme molecules immobilized on the surface brought 12% of the molecules to the native state (FRET ~ 0.9) and 88% to a misfolded state (M, FRET ~ 0.3) (23). As expected, the ribozyme molecules with FRET of ~ 0.9 had S cleavage activity, whereas the misfolded molecules did not (23). These results agree quantitatively with previous results from unmodified free ribozyme in solution, indicating that the folding process was not perturbed by surface immobilization and dye-labeling (18).

Time-resolved single-molecule FRET measurements allowed us to follow the folding dynamics. Figure 5A shows the FRET time trace of a molecule unfolding and refolding to

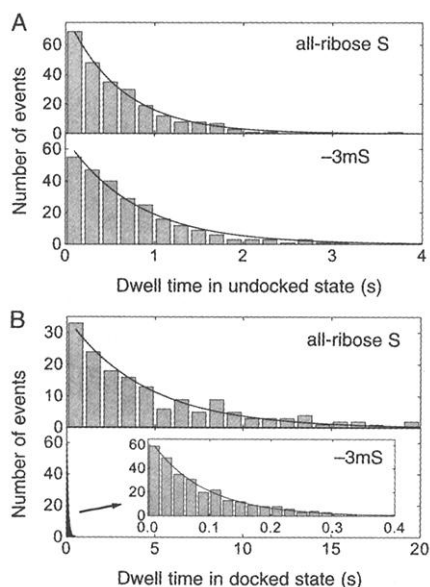


Fig. 4. Histograms of the dwell times in the undocked (A) and docked states (B) obtained from the FRET time-trajectories. The solid lines are single exponential fits of the data giving rate constants for docking and undocking, respectively, and their statistical errors. For the all-ribose S and the -3mS , k_{dock} is $1.62 \pm 0.08 \text{ s}^{-1}$ and $1.25 \pm 0.06 \text{ s}^{-1}$, respectively, and k_{undock} is $0.224 \pm 0.015 \text{ s}^{-1}$ and $11.5 \pm 1.0 \text{ s}^{-1}$.

the native state; Fig. 5B shows the histogram of folding times obtained from such time traces. The ribozyme folds with two distinct rate constants, 1.0 s^{-1} and 0.016 s^{-1} . Because of the short detection time, the conversion from M to the native state ($\sim 10^{-5} \text{ s}^{-1}$) was not observed here. The slow rate constant of 0.016 s^{-1} is the same as the previously established folding rate (13–15, 18), further demonstrating that the folding dynamics is not perturbed by surface immobilization and dye-labeling. The fast rate constant of 1.0 s^{-1} was not observed before and thus indicates the existence of a new folding pathway.

This fast-folding pathway depends on the presence of bound S during folding. In the single-molecule experiments, all detected ribozyme molecules were bound to S, and 35% of the molecules that reached the native state folded along the fast pathway. A similar fraction of ribozyme was ob-

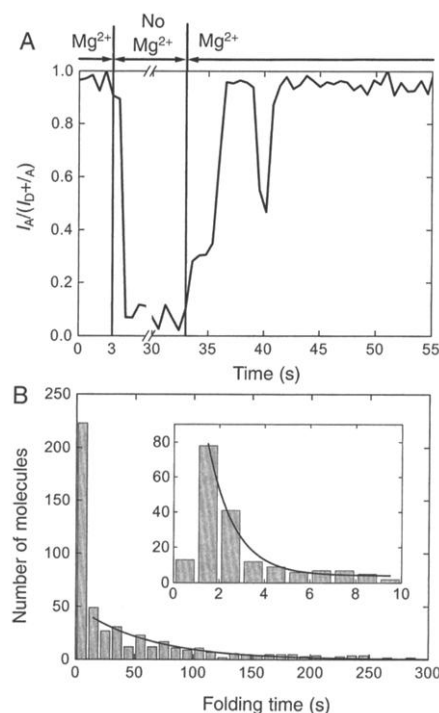


Fig. 5. (A) FRET time trace showing unfolding and refolding of a ribozyme molecule. The ribozyme was prefolded to the native state, immobilized, and then unfolded by adding buffer lacking Mg^{2+} at time = 3 s. After 30 s, a period long enough to ensure complete unfolding (23), a buffer containing Mg^{2+} was added to refold the ribozyme. The transient decrease at $\sim 40 \text{ s}$ is an undocking event. (B) Folding time histogram. The folding time is defined as the time between the addition of folding buffer and the FRET signal reaching 0.8 (48). The line is a single exponential fit to the data with the first bin excluded, giving a rate constant of $0.016 \pm 0.001 \text{ s}^{-1}$. (Inset) Expansion of the first bin of the main histogram. Relatively few molecules folded in the first second, due to a delay between the initiation of refolding buffer and its arrival at the sample. The line is a single exponential fit giving a rate constant of $1.0 \pm 0.3 \text{ s}^{-1}$.

served to fold rapidly ($>0.2 \text{ s}^{-1}$) in an ensemble experiment of free ribozyme in solution, in which most ribozyme molecules were bound to S at the onset of folding (23). No fast-folding fraction was observed when S was absent at the onset of folding (23), explaining why this fast-folding pathway was not observed previously.

At the early stage of folding, the FRET signal increased to and transiently stayed at ~ 0.3 (Fig. 5A), suggesting the existence of at least one intermediate folding state. Because of our slow buffer exchange ($\sim 1 \text{ s}$), the rate constant for formation of the intermediate can only be assigned a lower limit of 1 s^{-1} . The average dwell times at this FRET level are 1 s and 60 s for the previously mentioned fast- and slow-folding molecules, respectively. Thus, this FRET level reflects two distinct folding intermediates. The short-lived intermediate I_S could be an early state in folding or the undocked but otherwise folded state because the undocked state also gives FRET of ~ 0.3 and a rate constant for docking of 1.6 s^{-1} . The longer lived intermediate I_L is likely a trapped state that does not fold readily. Earlier studies have shown that an independent folding subdomain, P4–P6, forms early in folding (15); thus, P4–P6 is likely to be formed in I_S and I_L .

To summarize what we now know about the overall folding transition, the ribozyme folds to the native state (N) through at least three pathways, each with at least one intermediate state preceding the rate-limiting step. A previously unobserved fast-folding pathway A passes through an intermediate state I_S and folds to N with an observed rate constant of 1.0 s^{-1} . Pathway B passes through a different intermediate state I_L and folds to N with an observed rate constant of 0.016 s^{-1} . Pathway C passes through the misfolded M and folds to N very slowly with a rate constant $\sim 10^{-5} \text{ s}^{-1}$ (18). Pathways B and C are coincident in early folding steps and branch only late in folding (46). We found that a significant population of pathway A depended on the presence of bound S, and the partitioning between M and N was the same in the presence or absence of bound S. These observations suggest that pathway A also branches to form M and that the branches from pathways A and B to M occur from a common intermediate or from intermediates sharing key features that determine the partitioning. The misfolded state M is known to contain an alternative secondary structure, AltP3, compared with N (46, 47). The molecular features of I_S and I_L remain to be explored.

References and Notes

1. T. T. Perkins, D. E. Smith, S. Chu, *Science* **276**, 2016 (1997).
2. See for example, E. Neher and B. Sakmann, *Nature* **260**, 779 (1976).
3. J. T. Finer, R. M. Simmons, J. A. Spudis, *Nature* **368**, 113 (1994).

4. R. D. Vale *et al.*, *Nature* **380**, 451 (1996).
 5. H. Noji, R. Yasuda, M. Yoshida, K. Kinoshita, *Nature* **386**, 299 (1997).
 6. M. D. Wang *et al.*, *Science* **282**, 902 (1998).
 7. H. P. Lu, L. Y. Xun, X. S. Xie, *Science* **282**, 1877 (1998).
 8. M. Rief, M. Gautel, F. Oesterhelt, J. M. Fernandez, H. E. Gaub, *Science* **276**, 1109 (1997).
 9. M. S. Z. Kellermayer, S. B. Smith, H. L. Granzier, C. Bustamante, *Science* **276**, 1112 (1997).
 10. L. Tskhovrebova, J. Trinick, J. A. Sleep, R. M. Simmons, *Nature* **387**, 308 (1997).
 11. R. M. Dickson, A. B. Cubitt, R. Y. Tsien, W. E. Moerner, *Nature* **388**, 355 (1997).
 12. R. F. Gesteland and J. F. Atkins, Eds., *The RNA World* (Cold Spring Harbor Laboratory Press, Cold Spring Harbor, NY, 1993).
 13. D. W. Celander and T. R. Cech, *Science* **251**, 401 (1991).
 14. P. P. Zarrinkar and J. R. Williamson, *Science* **265**, 918 (1994).
 15. B. Sclavi, M. Sullivan, M. R. Chance, M. Brenowitz, S. A. Woodson, *Science* **279**, 1940 (1998).
 16. J. Pan, D. Thirumalai, S. A. Woodson, *J. Mol. Biol.* **273**, 7 (1997).
 17. D. K. Treiber, M. S. Rook, P. P. Zarrinkar, J. R. Williamson, *Science* **279**, 1943 (1998).
 18. R. Russell and D. Herschlag, *J. Mol. Biol.* **291**, 1155 (1999).
 19. T. Pan, *Biochemistry* **34**, 902 (1995).
 20. P. P. Zarrinkar, J. Wang, J. R. Williamson, *RNA* **2**, 564 (1996).
 21. X. Fang, T. Pan, T. R. Sosnick, *Nature Struct. Biol.* **6**, 1091 (1999).
 22. T. R. Cech and D. Herschlag, *Nucleic Acids Mol. Biol.* **10**, 1 (1996).
 23. Supplementary material is available at www.sciencemag.org/feature/data/1049406.shl.
 24. To assess the specificity of ribozyme binding, streptavidin-coated surfaces were incubated with ribozyme bound to biotinylated and non-biotinylated tethers. The former gave 100-fold greater surface density of fluorescently labeled molecules than the latter, demonstrating that the biotinylated ribozyme binds to the surface predominately through the biotin-streptavidin interaction.
 25. In the total internal reflection microscope, fluorescent molecules were excited by an evanescent wave generated by total internal reflection of a 514-nm laser beam and detected by a CCD (charge-coupled device) camera (23). The microscope could detect several hundred individual molecules simultaneously with a time resolution of 100 ms. The cleavage kinetics and overall folding kinetics were measured using this apparatus. In the scanning confocal microscope, fluorescent molecules were excited by a focused 514-nm laser beam and detected by avalanche photodiodes. This apparatus can measure the fluorescence emission of one molecule with a time resolution of 1 ms. The docking kinetics were measured using this apparatus.
 26. D. Herschlag and T. R. Cech, *Biochemistry* **29**, 10159 (1990).
 27. Bulk measurements were carried out by the conventional single-turnover radioactive assay (26). Ribozyme (100 nM) was bound to a trace amount (<1 nM) of 5'-[³²P]-labeled S. After ≥1 min for binding of S, cleavage was initiated by addition of G. Reactions measuring the rate constant for S binding were carried out as previously described (26).
 28. The identical k_{max} indicate that the ternary complex of ribozyme-S-G is unperturbed by the surface. Under the conditions used in the experiments, $K_{1/2}^G$ is equal to K_d^G , the equilibrium dissociation constant of G [T. S. McConnell, T. R. Cech, D. Herschlag, *Proc. Natl. Acad. Sci. U.S.A.* **90**, 8362 (1993)]; thus, the identical $K_{1/2}^G$ indicates that the G binding site is unperturbed by the surface.
 29. L. Stryer and R. P. Haugland, *Proc. Natl. Acad. Sci. U.S.A.* **58**, 719 (1967).
 30. G. J. Schutz, W. Trabesinger, T. Schmidt, *Biophys. J.* **74**, 2223 (1998).
 31. T. Ha *et al.*, *Proc. Natl. Acad. Sci. U.S.A.* **96**, 893 (1999).
 32. T. Ha *et al.*, *Proc. Natl. Acad. Sci. U.S.A.* **96**, 9077 (1999).

33. The FRET efficiency is given by $1/[1 + (R/R_0)^6]$, where R is the distance between the donor and acceptor. R_0 is typically between 3 and 7 nm, depending on the spectral overlap between the donor emission and acceptor absorption, quantum yield of the donor, and the orientations of the donor and acceptor. Thus, the FRET efficiency strongly depends on the distance between donor and acceptor as well as their orientations. Although there is a strong expectation of a large decrease in distance between the donor and acceptor upon P1 docking or overall folding, the conclusions here are independent of whether the FRET efficiency responds to changes in distance, orientation, or both.
 34. D. Herschlag, *Biochemistry* **31**, 1386 (1992).
 35. P.C. Bevilacqua, R. Kierzek, K. A. Johnson, D. H. Turner, *Science* **258**, 1355 (1992).
 36. J. A. Latham and T. R. Cech, *Science* **245**, 276 (1989).
 37. B. L. Golden, A. R. Gooding, E. R. Podell, T. R. Cech, *Science* **282**, 259 (1998).
 38. V. Lehnert, L. Jaeger, F. Michel, E. Westhof, *Chem. Biol.* **3**, 993 (1996).
 39. J.-F. Wang, W. D. Downs, T. R. Cech, *Science* **260**, 504 (1993).
 40. G. J. Narlikar and D. Herschlag, *Nature Struct. Biol.* **3**, 701 (1996).
 41. Previous studies of the rate constants for docking (35, 45), using different substrates under different conditions, yielded values within the same order of magnitude as reported here.
 42. A. R. Fersht, A. Matouschek, L. Serrano, *J. Mol. Biol.* **244**, 771 (1992).

43. A. M. Pyle, F. L. Murphy, T. R. Cech, *Nature* **358**, 123 (1992).
 44. D. Herschlag, F. Eckstein, T. R. Cech, *Biochemistry* **32**, 8299 (1993).
 45. G. J. Narlikar, L. E. Bartley, M. Khosla, D. Herschlag, *Biochemistry* **38**, 14192 (1999).
 46. R. Russell and D. Herschlag, unpublished data.
 47. J. Pan and S. Woodson, *J. Mol. Biol.* **280**, 597 (1998).
 48. To demonstrate that the ribozyme attains its native state when the FRET value reaches ≥0.8, ribozyme molecules were unfolded with a buffer lacking Mg²⁺ and refolded with a buffer containing 5 mM Mg²⁺ and 0.3 mM G. The time traces with FRET reaching ≥0.8 after refolding show simultaneous disappearance of both donor and acceptor signals within a few seconds, due to the cleavage of S. The histogram of the time between FRET reaching ≥0.8 and disappearance of fluorescence shows a single exponential decay with a rate constant of 0.25 s⁻¹, the same as the cleavage rate constant obtained from prefolded ribozyme.
 49. We are grateful to S. A. Scaringe and J. A. Orr for their advice on oligonucleotide preparation. This research was supported by an NSF grant (PHY-9970017) and an Air Force Office of Scientific Research grant (F49620-98-1-0219) to S.C. and an NIH grant (GM49423) to D.H. X.Z. was supported by the Chodorow Fellowship of the Stanford Applied Physics Department and an NIH postdoctoral fellowship. L.E.B. was supported in part by an NIH training grant. H.P.B. was supported in part by a Center on Polymer Interfaces and Macromolecular Assemblies grant. R.R. was supported by an NIH postdoctoral fellowship.

11 February 2000; accepted 28 April 2000

Role of CD47 as a Marker of Self on Red Blood Cells

Per-Arne Oldenborg,¹ Alex Zheleznyak,¹ Yi-Fu Fang,¹ Carl F. Lagenaur,² Hattie D. Gresham,³ Frederik P. Lindberg^{1*}

The immune system recognizes invaders as foreign because they express determinants that are absent on host cells or because they lack "markers of self" that are normally present. Here we show that CD47 (integrin-associated protein) functions as a marker of self on murine red blood cells. Red blood cells that lacked CD47 were rapidly cleared from the bloodstream by splenic red pulp macrophages. CD47 on normal red blood cells prevented this elimination by binding to the inhibitory receptor signal regulatory protein alpha (SIRPα). Thus, macrophages may use a number of nonspecific activating receptors and rely on the presence or absence of CD47 to distinguish self from foreign. CD47-SIRPα may represent a potential pathway for the control of hemolytic anemia.

Natural killer (NK) cells eliminate target cells recognized by a range of activating receptors that bind ligands on many normal cells. However, expression of self major histocompatibility complex (MHC) class I molecules can protect a cell by binding to NK cell inhibitory receptors, which recruit and activate src-homology phosphatases (SHP-1 and SHP-2)

that inhibit cell activation (1-4). NK cells thus spare cells that express "markers of normal self" in the form of MHC class I molecules, and eliminate them when these markers are absent or inadequately expressed. In contrast to what might be expected, MHC class I-deficient mice are not autodestructive. Rather, NK cell recognition adapts to the level of inhibitory ligand expressed in the NK cell environment (5). Expression of molecules related to NK cell inhibitory receptors on other leukocytes suggests that similar mechanisms are operative, for example, in macrophage activation (4, 6, 7). Although many of these molecules recognize MHC class I, the "marker of self" could in principle be any ubiquitously expressed surface molecule.

¹Division of Infectious Diseases, Department of Internal Medicine, Campus Box 8051, Washington University School of Medicine, 660 South Euclid Avenue, St. Louis, MO 63110, USA. ²Department of Neurobiology, School of Medicine, University of Pittsburgh, Pittsburgh, PA 15261, USA. ³Research Service, Albuquerque VA Medical Center, Albuquerque, NM 87108, USA.

*To whom correspondence should be addressed. E-mail: lindberg@id.wustl.edu